On the Meteorological Conditions during Postprecipitation Periods: Implications to Pollutant Dispersion

G. KALLOS

University of Athens, Department of Applied Physics, Athens, Greece

M. SEGAL

Department of Physics and Astronomy, University of Kansas, Lawrence, Kansas

(Manuscript received 18 January 1990, in final form 29 June 1990)

ABSTRACT

The various processes within the atmospheric boundary layer (ABL) during precipitation events tend to thermally stabilize the ABL. Selected observations are presented in order to illustrate this thermal stabilization for convective and stratified cloud systems. A tendency towards the onset of moist-adiabatic temperature profiles is suggested during stratified precipitation events. Conceptual, analytical, and numerical model evaluations were performed, suggesting that pollutant dispersion characteristics during the postprecipitation periods are likely to be modified considerably compared to these in the preprecipitation periods. When a moist-adiabatic temperature profile is generated as a result of a precipitation event, the significance of the impact on pollutant dispersion under light wind conditions is dependent on the environmental background temperature, where in a warm environment the reduction in pollutant dispersion is most pronounced. Thermal circulations related to cool air pools typical of postprecipitation events and their implications to pollutant dispersion were evaluated by illustrative numerical model simulations. The simulation results imply that the reduction of postprecipitation turbulence effect, due to thermal stabilization of the ABL, may be offset in many situations by the thermal circulations mostly when convective precipitation is involved. Differences between the daytime and nocturnal development of these circulations were found to be significant.

1. Introduction

Following the passage of a relatively large convective storm system with associated precipitation activity, a cool and stable air pool with a typical horizontal scale of tens to a few hundred kilometers, often is formed in the lower atmosphere due to droplet-evaporative cooling and downdrafts (e.g., Fujita 1955; Atkinson 1981; Hamilton and Johnson 1987). Likewise, as a result of precipitation related to stratiform cloud systems, similar thermal modifications of the lower atmosphere are produced (e.g., Wesley and Pielke 1990). In most observational documentation of those modifications in the lower atmosphere, interest has focused on the atmospheric environment during the precipitation period, and little information is available about the postprecipitation atmospheric environment (i.e., more than 50–100 km to the rear of the passing storm). The postprecipitation stable cool air pool is gradually modified following the passage of the weather system as a result of the boundary layer thermal processes, while the horizontal thermal contrast associated with the cool air pool and its surroundings provide forcing for thermal flows similar to sea breezes.

Similar characteristics as described previously, though not so pronounced, may be observed following isolated convective precipitation events (i.e., horizontal scales not larger than several tens of kilometers). Following the precipitation period, the vertical profile of temperature in such events would tend toward the wet-bulb temperature. However, this temperature structure is likely to be distorted by downdraft circulations.

When large-scale precipitation related to stratiform clouds is considered (as typical in winter in the mid-latitudes), the downdraft intensity is reduced. Consequently, a tendency toward establishing more defined thermal stratification associated with relatively light winds is more likely compared to that associated with convective cloud precipitation.

The aforementioned impacts of precipitation processes on the lower atmosphere are anticipated to modify local pollutant-dispersion conditions over a period of several hours; and for longer periods in the absence of any significant changes in the synoptic conditions. For example, a change from the commonly observed deep summer daytime convective atmospheric boundary layer (ABL) into a stable ABL during, and immediately following, the precipitation event

Corresponding author address: Dr. George Kallos, Department of Applied Physics (Meteorology), University of Athens, Ippokratous 33, Athens 10680, GREECE.

will affect dispersion by reducing the turbulence intensity. On the other hand, this effect may be offset due to the strong wind (i.e., increased ventilation), as well as wind shear in the postprecipitation lower atmosphere. Worth noting, however, is that during intense precipitation events, washout of atmospheric aerosol pollutants and soluble gases is likely to reduce significantly their background concentration level.

The modifications in the lower-atmosphere flow conditions and thermal stratification during and following precipitation events are suggested, at least occasionally, to be substantial. However, apparently no specific attention has been given to their implication to pollutant dispersion conditions. The present study is an attempt to provide *preliminary* evaluation in this direction using scaling, observational, and modeling approaches. The evaluations are involved with situations in which the thermal stratification is not determined by frontal passage. A selective observational illustration of the impact of precipitation events on the lower-atmospheric thermal stratification is given in section 2. Selective general evaluations of pollutant dispersion characteristics involved with an extended area affected by precipitation are given in section 3. The postprecipitation thermally induced circulations and their significance to pollutant dispersion are examined through illustrative model simulations in section 4. A discussion of the possible impacts of precipitation events on pollution-dispersion potential, based on evaluations provided in this study, is given in section 5.

2. Observations of the effect of precipitation systems on the thermal structure of the atmosphere

Illustrative observations of the thermal stratification (including temperature T and dewpoint temperature T_d) associated with precipitation events and postprecipitation are provided in the following discussion. The database consists of profiles reported in various studies (partially referenced in this section and in section 4) and selective NWS radiosonde data collected during a period of two years (1987–88). Convective and stratiform precipitation events are considered. The presented illustrations reflect general features and trends of modified thermal stratification, however, variations from these features should not be regarded as infrequent. Also, it is worth noting that for generality the presented radiosonde profiles cover most of the depth of the atmosphere. However, for dispersion evaluations, in most cases, only the lower 1 km of the atmosphere is pertinent.

a. Convective cloud system precipitation

The vertical extent of the cool air pool, in the rear of summer storms, is typically a few hundred meters to 1 km, in which the air is near saturation and occasionally stable (e.g., Fujita 1955; Zipser 1977; and Johnson and Hamilton 1988 among others). Above this cool air pool, in many cases, there is a relatively warm and dry air layer (rear inflow) sometimes extending up to about 600 mb (see Johnson and Hamilton 1988). Above this layer, the atmospheric lapse rate is, in most cases, near the moist adiabatic up to the tropopause. This feature of the temperature profile was presented in the observational study by Zipser (1977) and is termed "the onion" or "the diamond" because of the combined shape of the temperature and dewpoint temperature soundings. An example of this situation is provided in Fig. 1a by presenting three soundings that were taken at Russell, Kansas, during an MCC event. The 1600 CST sounding provides the thermal stratification at the commencement of the storm; the 1800 CST sounding shows the conditions during the storm, while the 2100 CST sounding shows the poststorm thermal characteristics. The first two soundings indicate a nearly moist-adiabatic lapse rate aloft, while the poststorm sounding indicates a very stable and saturated layer near the ground with the dry and warmer layer above reaching to $\approx$600 mb.

b. Convective–stratiform cloud system precipitation

Figure 1b presents the temperature profiles during an extended summer precipitation event along the Front Range of Colorado. The general profile feature, during the period of observation, is nearly moist adiabatic in the lower layers with near-surface stabilization. During the precipitation event, presented in Fig. 1c, the thermal stratification in the lower atmosphere tended to be nearly moist adiabatic. Weather maps for the cases presented in Figs. 1b,c suggest that the precipitation events were associated with the "mixture" of convective and stratiform type clouds. In both cases, a weak surface pressure low was observed along the Front Range of Colorado with a ridge at 500 mb. Rain and light surface winds were reported in an extended area east of the Rocky Mountains.

c. Stratiform cloud system precipitation

Figure 1d presents profiles of T and T_d during a snowfall event in Denver, Colorado, indicating the establishment of nearly moist-adiabatic thermal stratification in the lower 1.5 km with air close to saturation. A capping inversion is noticeable above this layer. The daily synoptic maps from NWS indicate light upslope flow along the Front Range of Colorado associated with a low pressure system with the center over New Mexico. Similar features of T and T_d during a snow storm along the Colorado Front Ridge are presented by Wesley and Pielke (1990).

Temperature profiles during two precipitation events taken in the Boulder Atmospheric Observatory (BAO) meteorological tower are presented in Figs. 2a,b. Based on the weather maps and surface observations for these days, rain was observed over a large area east of the Rocky Mountains. Stratiform clouds and periodic light

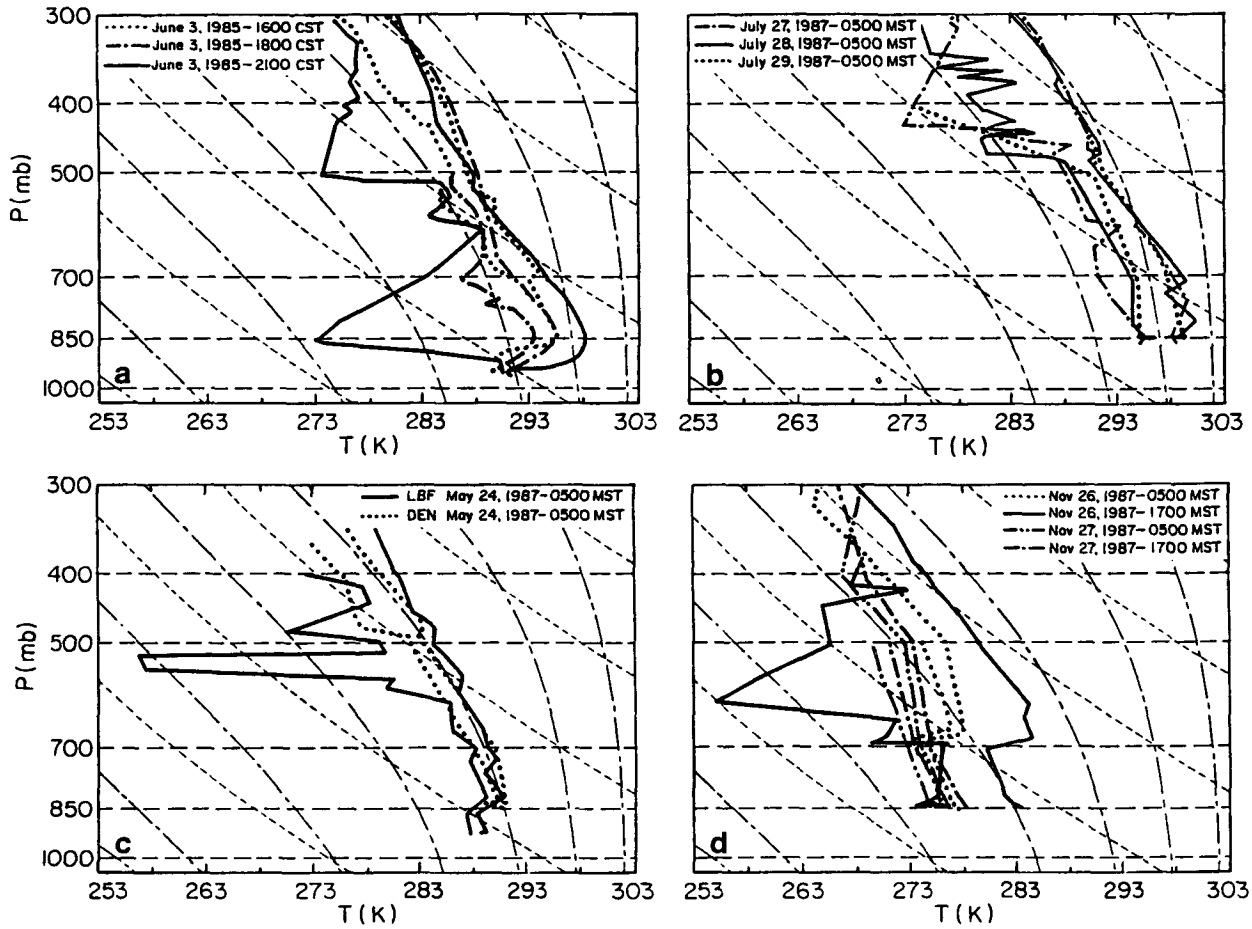

FIG. 1. Illustrative temperature and dewpoint temperature profiles on a skew-T diagram: (a) involved with MCC at Russell, Kansas, reproduced from Fortune (1989); (b) at DEN (Denver, Colorado) during summer precipitation events; (c) at DEN and LBF (North Platte, Nebraska) during spring precipitation events; and (d) at DEN, during winter snowfall event.

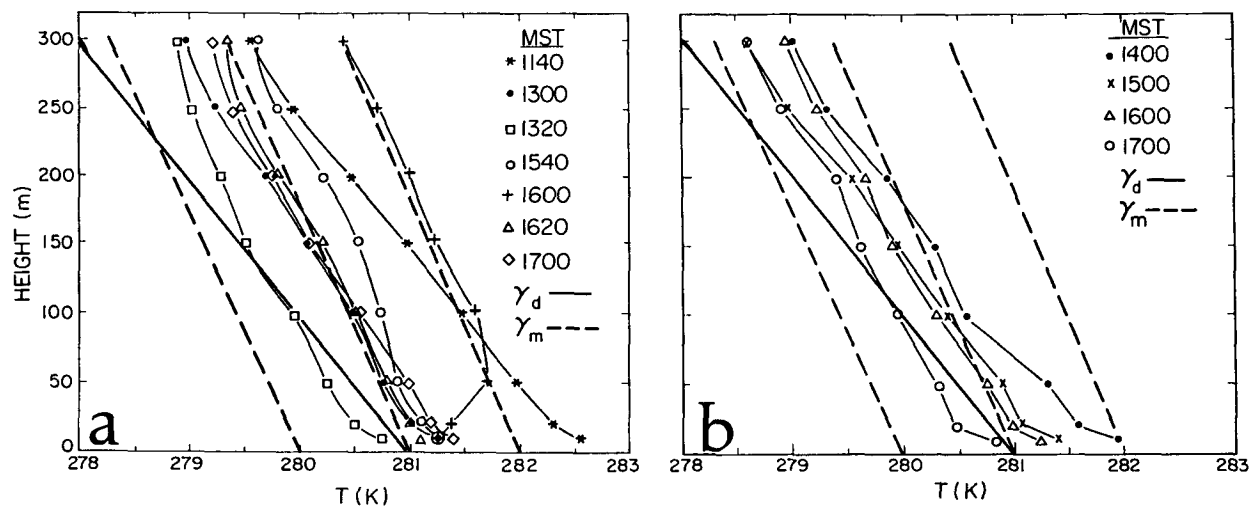

FIG. 2. Illustrative temperature profiles at the BAO (Boulder Atmospheric Observatory) meteorological tower (a) 21 May 1987; and (b) 13 September 1988. Here γ_d and γ_m indicate the dry-adiabatic and moist-adiabatic temperature lapse rates, respectively.

rain were reported in the Boulder area during the presented days. Generally, the winds during both events were light at the tower measurement levels (in the range of 1–5 m s^{-1}). The temperature profiles during these events tended toward the moist adiabatic.

Near-surface temperature inversion was observed for a short period of time (Fig. 2a; 1600 MST). Similar temperature profile patterns were also observed in additional rain events in this area. Typically, in clear days during this period of the year, slightly superadiabatic temperature profiles are observed in association with a well-developed mixed layer at the BAO (not shown).

d. Some generalizations

Commonly the preprecipitation period in midlatitudes is associated with a daytime convective ABL, the depth of which depends mostly on the magnitude of the surface sensible heat fluxes as well as on the early morning lower-atmosphere thermal stratification. Therefore, the ABL depth can be related to factors such as season, geographical location, land use, and prevailing synoptic conditions. General climatology of the ABL characteristics in the United States is given in Holzworth and Fisher (1979); studies for specific sites are available, for example, in Haagenson (1979).

Based on the evaluations made previously (supported by representative illustrations and pertinent documentation), the following is suggested: (i) when an extended area is affected by precipitation, the lower atmosphere tends frequently to become thermally stabilized and, in many cases, acquires a temperature profile at least as the moist adiabatic. Towards the end of the event, further thermal stabilization may be observed in a layer of typical depth of a few hundred meters. (ii) In the lowest few tens of meters above the surface, temperature inversions may be established temporarily. Subsequently, in the case of an extensive area affected by precipitation, daytime supply of sensible heat flux into the atmosphere leads to a gradual reestablishment of the convective ABL. Reduction in the development of the ABL is likely to result (during the daytime) from suppression of the surface sensible heat fluxes forced by: (i) moistening of the ground by the precipitation (e.g., specific evaluations in Segal et al. 1990) and (ii) cloud shading.

In the following section, general evaluations as well as numerical model estimations of precipitation impact on meteorological fields related to pollutant dispersion potential are provided.

3. Dispersion evaluation over an extended area affected by uniform precipitation

As suggested in the previous section, the postprecipitation lower atmosphere, in many cases, is likely to acquire at least moist-adiabatic thermal stability. The evaluations presented in the following are made while assuming moist-adiabatic temperature profiles (unless stated otherwise, the atmosphere is assumed to be subsaturated) and, therefore, estimating the minimum effects of precipitation events on the ABL development and turbulence. Evaluation of the modifications involved with more stable stratification can be easily deduced based on the presented formulation.

a. Dispersion under saturated moist-adiabatic atmospheric stratification

Assume that a saturated *moist*-adiabatic atmospheric stratification exists during a light rain event while the cloud-induced dynamical effects, within the ABL, are small. In this situation, turbulence processes are involved with *neutral thermal stratification.* When an air parcel is displaced by turbulence, upward or downward, a change in the parcel temperature along the moist adiabatic curve is assumed (for the downward motion it is applicable when the droplet's evaporation is sufficient to compensate for the departure from saturation as the air parcel descends). Therefore, the average upward and downward turbulence motions are the same, as illustrated schematically in Fig. 3a. In contrast, for the case of a *nonprecipitating* saturated moist-adiabatic atmosphere, the turbulent parcel moving upward will be associated with neutral stratification dispersion characteristics, while turbulent parcels involved with downward motion will be affected by stable atmospheric dispersion conditions (Fig. 3b). Thus, the vertical dispersion characteristics are likely to be nonisotropic. Following the precipitation event, the relative humidity decreases gradually from 100%. The thermal stratification, on the other hand, may remain stable and close to the moist adiabatic temperature profile. Therefore, pollutant dispersion within the layer of interest will be reduced in comparison to the previous situations (Fig. 3c).

b. The impact of background temperature level

In the following a postprecipitation moist-adiabatic temperature profile associated with a subsaturated atmosphere is assumed. The moist-adiabatic potential temperature rate, γ_m, depends on the air temperature T and the pressure P through the relation (e.g., Iribarne and Godson 1981):

$$\gamma_m = \gamma_d\left(1 + \frac{0.622 L e_s}{R_d T P}\right)\left(1 + \frac{0.622^2 L^2 e_s}{C_{pd} R_d T^2 P}\right)^{-1} \quad (1)$$

where L is the latent heat of water-vapor condensation, R_d is the gas constant, C_{pd} is the specific heat of the dry air in constant pressure, e_s is the saturation vapor pressure, and γ_d is the dry-adiabatic temperature lapse rate (9.8 K km^{-1}). For near-surface pollutant dispersion (in this study P_{surface} = 1000 mb) a range of air temperature within 253 to 313 K was considered; the corresponding values of γ_m are given in Fig. 4. The

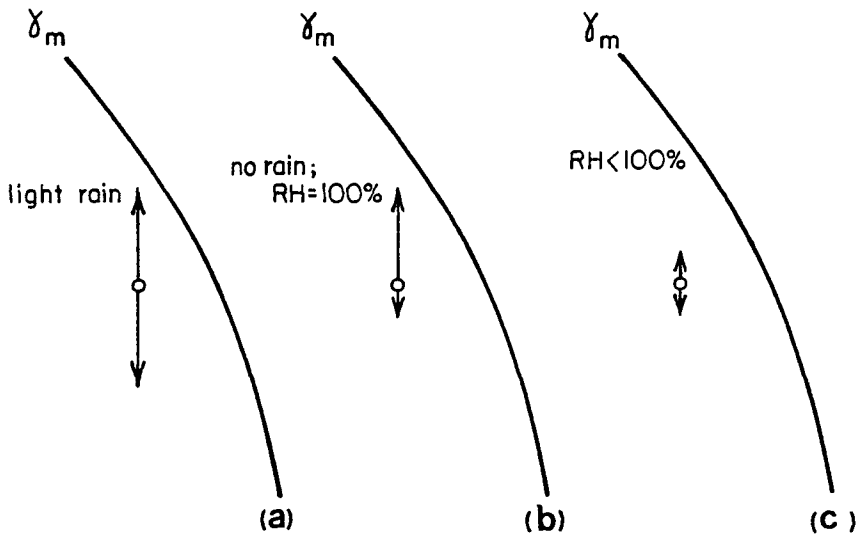

FIG. 3. Schematic illustration of the extent of upward and downward air parcel movements by turbulence (as indicated by the arrows size) in moist-adiabatic stratification: (a) under light rain conditions; (b) under no-rain saturated air conditions; and (c) under subsaturated air conditions.

change in γ_m, within this range of temperatures, is quite significant, increasing from about 1.2 K km^{-1} at 253 K to 6.7 K km^{-1} at 313 K. Obviously, for very low temperatures (such as those involved with cold air masses or those typical of the high latitudes during the winter), $\gamma_m \rightarrow \gamma_d$, therefore, some improvement in dispersion conditions, compared with these in higher temperature environments, should be anticipated.

The corresponding changes in stability classes, in the context of the σ dispersion curves and due to the dependence of γ_m on the background temperatures, are also illustrated in Fig. 4 by adopting the Carpenter et al. (1971, p. 497) classification. As evident from the illustration, γ_m corresponds to a "neutral" dispersion class in the 255 K environment and to a "stable" dispersion class in the 283 K environment. Similarly, the related modifications in the computed plume rise can be estimated. In order to provide a qualitative estimation of the dependence of high stack plume rise on background temperature, the Briggs (1975) plume-rise formula was utilized under stable conditions:

$$\Delta h_s = 5F_o^{1/4}(g\beta_o/\theta_o)^{-3/8} \qquad (2)$$

where F_o is the plume buoyancy at the stack top, g is the gravity acceleration, θ_o is a reference potential temperature, and β_o is the potential temperature lapse rate.

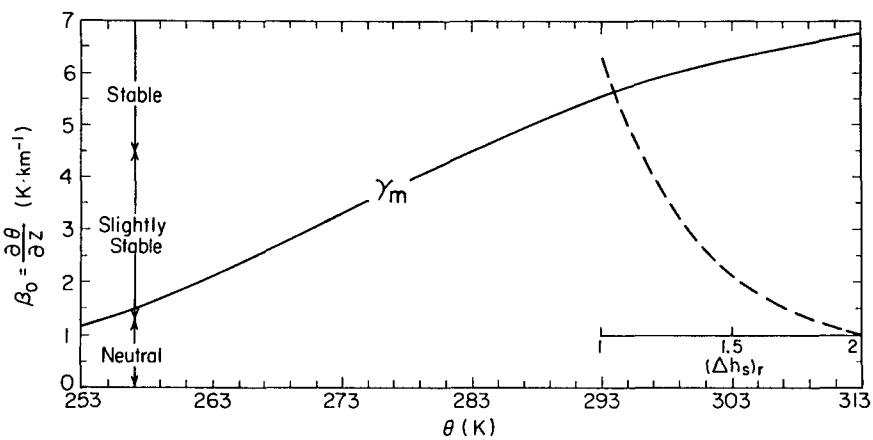

FIG. 4. The dependence of the moist-adiabatic lapse rate, γ_m, on the background potential temperature, θ, (solid-line), and the related impact of change in γ_m on atmospheric stability dispersion classes (based on Carpenter et al. 1971). The relative change in plume rise above tall stack, $(\Delta h_s)_r$, within the range of changes in γ_m (with reference γ_m at 303 K), is illustrated by the dashed line.

Assuming that the plume rise for $\beta_o = \gamma_m = 6.5$ K km^{-1} (i.e., background temperature of 303 K) is Δh_s, the relative increase in Δh_s, $(\Delta h_s)_r$, as γ_m reduces under the same emission parameters, is shown by the dashed curve in Fig. 4. When the background temperature is reduced to 253 K, $(\Delta h_s)_r$ is increased by a factor of almost 2.

c. *Postprecipitation development of the ABL*

Assume a precipitation event over an extended domain that results in a moist adiabatic temperature lapse rate, γ_m, within the lower atmosphere. The characteristics of the newly established daytime convective ABL, as dependent on the background temperature, is an important parameter in air pollution evaluations. General estimation of this situation is given using a scaling approach. Illustrative cases are provided using numerical model computations. It is assumed that the affected area is extensive enough that conditions are horizontally homogeneous on the local scale, thus, permitting one-dimensional simulations.

1) ANALYTICAL RESULTS

In order to provide general scaling for the impact of the background temperature level on the development of daytime ABL, the following approximations are adopted. The depth of the daytime ABL, h_t, at time, t, following the initiation of sensible heat fluxes into the atmosphere is estimated by (e.g., Tennekes 1973):

$$h_t \approx \left[\frac{2 \int_o^t H_s dt}{\rho C_p \beta_o} \right]^{1/2} \tag{3}$$

where ρ is the air density and H_s is the surface sensible heat flux. The potential temperature lapse rate within the lower atmosphere, β_o, is assumed to be equal to γ_m at sunrise.

In the present study, it is assumed that at time t following sunrise and for clear sky conditions:

$$H_s = H_{s_o} \sin(\pi t/D) \tag{4}$$

where H_{s_o} is the noon-hour value of H_s and D is the duration of sunshine. Substituting Eq. (4) into Eq. (3) results in:

$$h_t = \left\{ \frac{2(D/\pi) H_{s_o} [1 - \cos(\pi t/D)]}{\rho C_p \gamma_m} \right\}. \tag{5}$$

Using the so-called combination formulation (Penman 1956) and following the approach discussed in Monteith (1981), H_{s_o} can be expressed for very wet ground (also see Segal et al. 1989b) as:

$$H_{s_o} = \frac{\Gamma}{s + \Gamma} (R_{N_o} - G_o) - \frac{\Gamma}{s + \Gamma} \frac{\rho L \delta q_a}{r_a} \tag{6}$$

where

R_{N_o} = the surface net radiation at noon
G_o = the surface soil fluxes at noon
$s = dq_s(T_S)/dT$, with $q_s(T_S)$ the saturated specific humidity at the surface temperature T_S
$\Gamma = C_p/L$ is the psychrometric constant
δq_a = the specific humidity deficit at the reference level in the air
r_a = the bulk aerodynamic resistance to water-vapor transfer (assumed the same as for heat transfer) between the surface and reference level z.

In Eq. (6) the first term of the rhs is the energy term and the second term represents the aerodynamical effects on H_{s_o}.

Equations (5) and (6) suggest that for *wet ground* conditions, the relative growth of h_t, as dependent on background potential temperature, θ, while assuming surface layers with the same values of $(R_{N_o} - G_o)$, δq_a and r_a, can be expressed through the factor $\eta(\theta)$ as:

$$\eta(\theta) = \left[\left(\frac{\Gamma}{\Gamma + s} \right)^{1/2} \gamma_m^{-1/2} \right]_\theta \left[\left(\frac{\Gamma}{\Gamma + s} \right)^{1/2} \gamma_m^{-1/2} \right]_{\theta_o}^{-1} \tag{7}$$

where θ_o is the reference potential temperature.

Figure 5 provides the dependence of η on θ (where θ is a representative potential temperature near the surface during the daytime) in the range of 273–308 K and with reference potential temperature $\theta_o = 308$ K. As evident from this figure, for wet surface conditions, namely, an initial moist-adiabatic θ profile in a relatively cold environment (273 K), the depth of the ABL is twice as large as that obtained under a relatively warm environment (298 K).

2) NUMERICAL MODEL EVALUATIONS

The formulation of the numerical model adopted for the evaluations given in the present study is provided in detail in Mahrer and Pielke (1977) and McNider and Pielke (1981) and, therefore, is not repeated here. The model was validated extensively

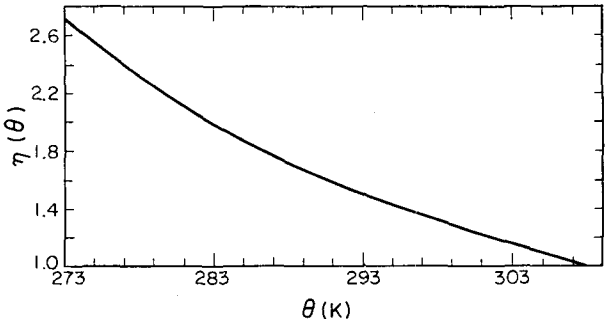

FIG. 5. The dependence of η [as defined in Eq. (7)] on the background potential temperature, θ.

against observations (e.g., Segal et al. 1982; Abbs and Pielke 1986; and Steyn and McKendry 1988, among others). A one-dimensional version of this numerical model was used in order to provide illustrative examples of the development of the daytime ABL following a precipitation event. The simulations were initialized by the average December and July minimum temperatures adopted from the *Climatic Atlas of the United States* (1968) with a corresponding moist adiabatic potential temperature lapse rate (see also Table 1 in Segal et al. 1989b). Six latitudes (25°, 30°, 35°, 40°, 45°, and 50°N) were considered along the central United States (95°W long). A list of the model input parameters is given in Table 1. The simulations were carried out for a ground wetness range from extremely dry to saturated. The dry ground conditions are assumed to be related to a light precipitation over dry ground (e.g., light precipitation following a prolonged drought). On the other hand, the saturated ground conditions are assumed to be associated with a heavy rain event. The surface wetness is expressed through the surface moisture availability m, which is defined as:

$$m = E/E_p, \tag{8}$$

where E and E_p are the actual and the potential evaporation rates at the surface, respectively. Worth noting is that Hanna and Paine (1989) found maximum surface concentrations from tall stacks could vary by a noticeable amount depending on the ground moisture. Segal et al. (1990) indicated the importance of the surface wetness effect on early and late daytime hours pollutant dispersions.

TABLE 1. Model input parameters and initial conditions.

Parameter		Value
General		
Surface roughness:		0.04 m
Soil specific heat:		1330 J kg^{-1} K^{-1}
Soil density:		1500 kg m^{-3}
Soil conductivity:	for $m \leq 0.2$	3×10^{-7} m^2 s^{-1}
	for $m > 0.2$	6×10^{-7} m^2 s^{-1}
Surface albedo:		0.2
Model levels = 5, 10, 20, 30, 40, 50, 75, 100, 200, 300, 400, 500, 600, 700, 800, 900, 1000, 1200, 1400, 1600, 1800, 2000, 2500, 3000, 3500, 4000, 4500, 5000, 5500, 6000, 7000, 8000, 9000, and 10 000 m.		
		1D simulations
Initial surface temperature:		December and July averaged daily temperature at 95°W long for the indicated latitude as given in *Climatic Atlas of the United States* (1968)
Initial $\partial\theta_0/\partial z$:		$\partial\theta_0/\partial z = \gamma_m$
Initial specific humidity:		85% relative humidity
Synoptic flow:		3 m s^{-1}
Beginning of the simulation:		0600 LST
Day of the year:		15 December (winter case) and 15 July (summer case)
		2D simulations
Initial $\partial\theta_0/\partial z$:		As shown in Figs. 8a,b
Initial specific humidity:		85% relative humidity
Synoptic flow:		(i) 0.5 m s^{-1} perpendicular to the domain cross section (ii) 3 m s^{-1} along the domain cross section
Beginning of the simulation:		1200 LST or 2000 LST
Day of the year:		(i) 15 August for summer simulations (ii) 15 December for winter simulations
Δx		6 km
Δt		30 s

The simulated height of the ABL, h, at 1500 LST, as dependent on the surface moisture availability m and latitude, under clear sky conditions for the winter (mid-December solar conditions) and for the summer (mid-July solar conditions), is presented in Figs. 6a and 7a, respectively. By analyzing the features presented in these figures, the following features are indicated:

(i) Moistening the soil contributes to a reduction in the value of h due to reduction in sensible heat flux.

(ii) The decrease in solar radiation while moving poleward (most significantly in the winter simulations) contributes to a reduction in the values of h. However, this impact is partially offset by the causes described in (iii) and (iv) below. Consequently reduction in h is simulated for latitudes higher than 45°N.

(iii) The climatological decrease of the air temperature while moving northward during the winter suggests, based on Fig. 4, a significant decrease in the value of γ_m (which is assumed to be the initial temperature stratification in the model simulations). The reduction in γ_m is *conducive* to a relatively significant enhancement of the daytime development of the ABL following a precipitation event, which results in a moist adiabatic temperature profile.

(iv) The climatological decrease of the air and surface temperatures while moving poleward results in a significant increase in the Bowen ratio (i.e., increase in the efficiency of converting net available radiation energy into sensible heat flux) and, consequently, contributes to an increase in the values of h (see detailed evaluations of this effect in Segal et al. 1989b). The scaled impact of the combined forcing involved with (iii) and (iv) on the value of h, as based on Eq. (7), is illustrated in Fig. 5.

Figures 6b and 7b present the same situations described in Figs. 6a and 7a, respectively, except that the incoming solar radiation reaching the surface was reduced by 50% (i.e., due to postprecipitation cloudi-

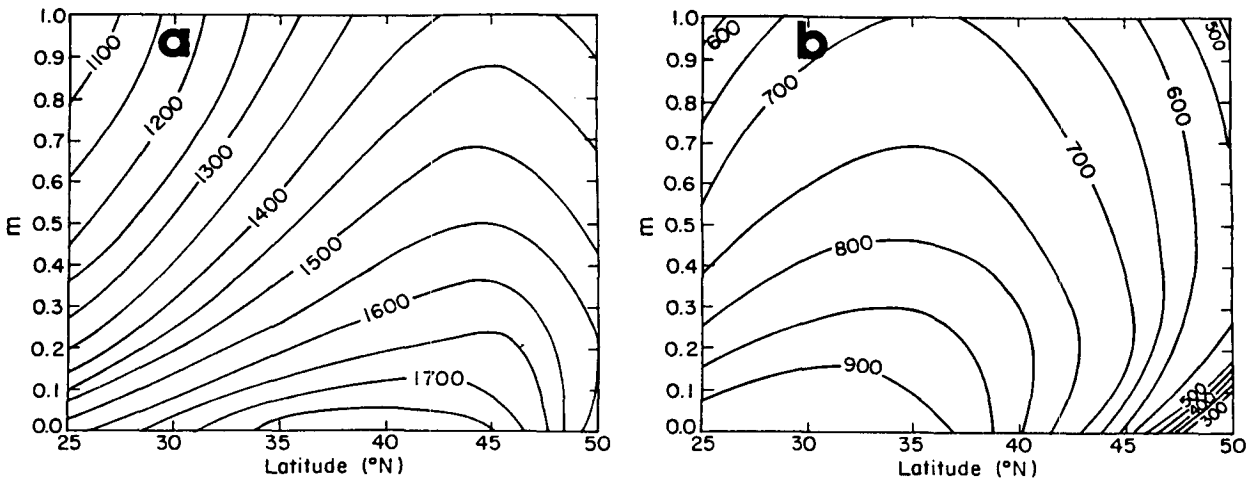

FIG. 6. Simulated ABL depths (in meters) at 1500 LST as dependent on surface moisture availability m and latitude, for 15 December sun conditions: (a) under clear sky conditions; (b) assuming reduction of the incoming solar radiation at the surface by 50% due to cloudiness.

ness). Similar general features to those obtained previously are found; although, as anticipated, the simulated depths of the ABL were reduced.

4. Thermally induced circulations

The mesoscale thermally induced circulations developed in the postprecipitation period as a result of the precipitation evaporative downdrafts cooling, obviously depend on the extent of the area affected by precipitation and the magnitude of the related temperature reduction as compared to that of the surroundings. The induced circulations can be compared to a sea breeze, although on some occasions they are likely to arise from stronger thermal forcing. Observational estimations of the decrease in the temperature following summer storms are reported in various studies. Wakimoto (1982) reported drops of $\approx$3–4 K within 1.3–4 km above ground. Garratt et al. (1985) observed drops of $\approx$5–9 K within a layer of 2–4 km above ground. Mahoney (1988) provides a variety of cases in which the drop in temperature is 1.4–4.7 K within depths of $\approx$1 km above ground. In most of the studies, the reported wind speeds are typically $\geqslant$10 m s^{-1} near the storm outflow region; although as the storm passes, usually the wind speed tends to reduce. A summary of the horizontal thermal contrast and the depth involved with sea-breeze circulations is given, for example, in Atkinson (1981) and Segal et al. (1989a). Typically, it is somewhat less pronounced compared to those previously suggested for the postprecipitation period.

Several illustrative simulations using a two-dimensional version of the numerical model were carried out in order to illustrate and scale the thermally induced circulations in the postprecipitation period. Table 1

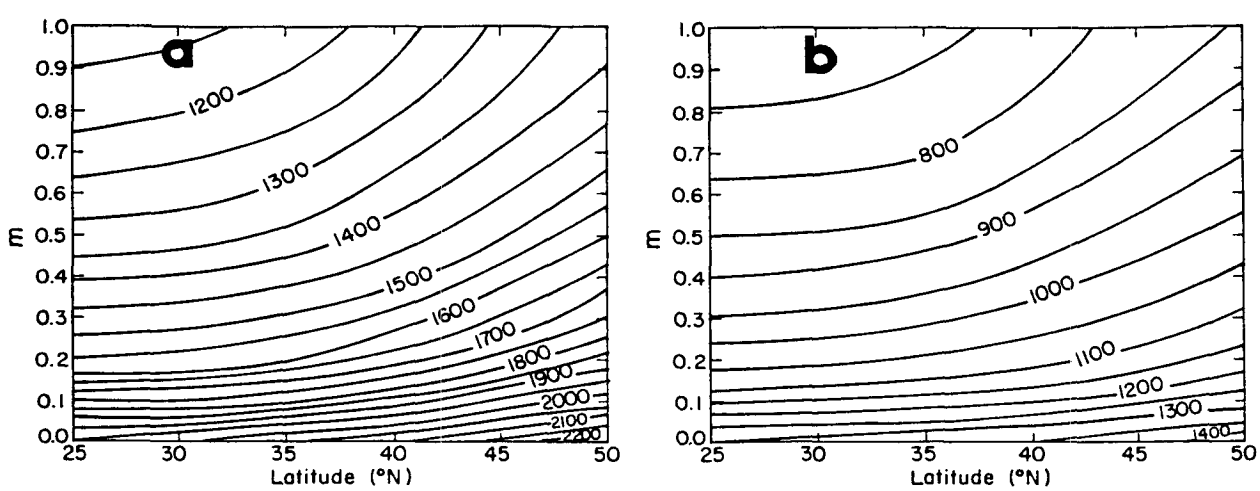

FIG. 7. The same as Fig. 6, except for the 15 July sun conditions.

TABLE 2. Brief description of the 2D simulations. The surface wetness conditions along the cool air pool are indicated as dry (m = 0.05) and wet (m = 0.5).

Simulation	Description
C1	wet; u_g = 0.5 m s^{-1}; starting hour—1200 LST; initial θ—Fig. 8a
C2	dry; u_g = 0.5 m s^{-1}; starting hour—1200 LST; initial θ—Fig. 8a
C3	wet; u_g = 3 m s^{-1}; starting hour—1200 LST; initial θ—Fig. 8a
C4	wet; u_g = 0.5 m s^{-1}; starting hour—1200 LST; initial θ—Fig. 8b
C5	wet; u_g = 0.5 m s^{-1}; starting hour—2000 LST; initial θ—Fig. 8a
C6	wet; u_g = 3 m s^{-1}; starting hour—2000 LST; initial θ—Fig. 8a

provides the input parameters for the model simulations, while Table 2 gives a brief description of the various simulations (which are labeled cases C1 to C6). The simulations were initiated by imposing a temperature perturbation reflecting the observations reported previously. The initial θ field was prescribed, assuming a pool of cool air, with a moist-adiabatic temperature profile at the center of the domain warming up gradually while being modified towards a neutral stratification. Two initial cool air pools were considered: (a) potential temperature perturbation for summer case simulations (Fig. 8a); and (b) for an illustrative winter case simulation (Fig. 8b). The initial pressure perturbation was computed by using the hydrostatic equation. The results of the simulations are presented in the following subsections.

a. Daytime simulations

These simulations were initiated at 1200 LST using the θ field described in Fig. 8a (clear sky conditions were assumed). For case C1, which is involved with a negligible background flow and wet ground at the cool-air section of the domain (i.e., as a result of intense precipitation there), the simulated u, v, and θ fields are presented in Fig. 9. By 1800 LST the u component has reached a maximum value of 4 m s^{-1} with a small v component established due to flow veering caused by the Coriolis force (Figs. 9a,b). The cool-air core has preserved its thermal contrast with the air over the surrounding dry area, due to suppression of the sensible heat fluxes over the wet ground section (Fig. 9c). It is associated with subsidence induced near the middle of the domain similar to that over the sea with a sea-breeze circulation. By midnight, the veering of the flow due to the Coriolis force (i.e., inertial oscillation) produced a noticeably larger v component compared to the u component (Fig. 9d,e). This veering of the thermally induced flow caused a reduced horizontal spread of the cold air mass and, therefore, aids in preserving its characteristics. Onset of a significant stable layer within the lowest 500 m, as a result of merging the surface nocturnal inversion with the upper capping inversion, is evident (Fig. 9f). Case C2 (Fig. 10) is the same as case C1 except for a relatively dry ground along the cool air pool location (i.e., a situation that is associated with light precipitation, causing stabilization of the ABL, although it is insufficient to cause changes in the ground moisture, which was initially assumed to be small). As a result of the enhanced surface sensible heat flux, the suppression of the cool air pool is faster than in the previous case. The reduction in the intensity of the circulation compared to that in case C1 is noticeable and is most pronounced in the 1800 LST fields (Figs. 10a–c), explained by the lack of the supportive thermal forcing due to horizontal surface moisture gradients, as in case C1. Development of a relatively deep daytime ABL within the cool air is evident (Fig. 10c). The circulation in the nocturnal period acquired a similar depth and horizontal extent as in the previous case, although the flow is somewhat weaker (Figs. 10d,e). The thermal stratification of the lower atmosphere is less stable (Fig. 10f) compared to the previous case.

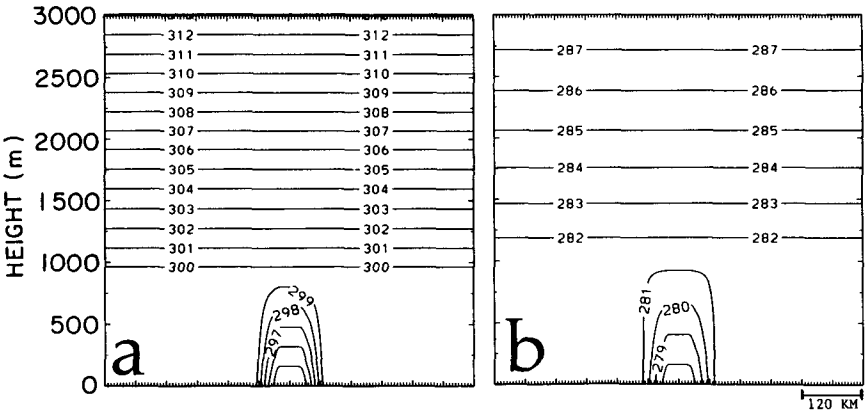

FIG. 8. The initial x–z potential temperature, θ (K) field used in the 2D model simulations (a) summer case; and (b) winter case.

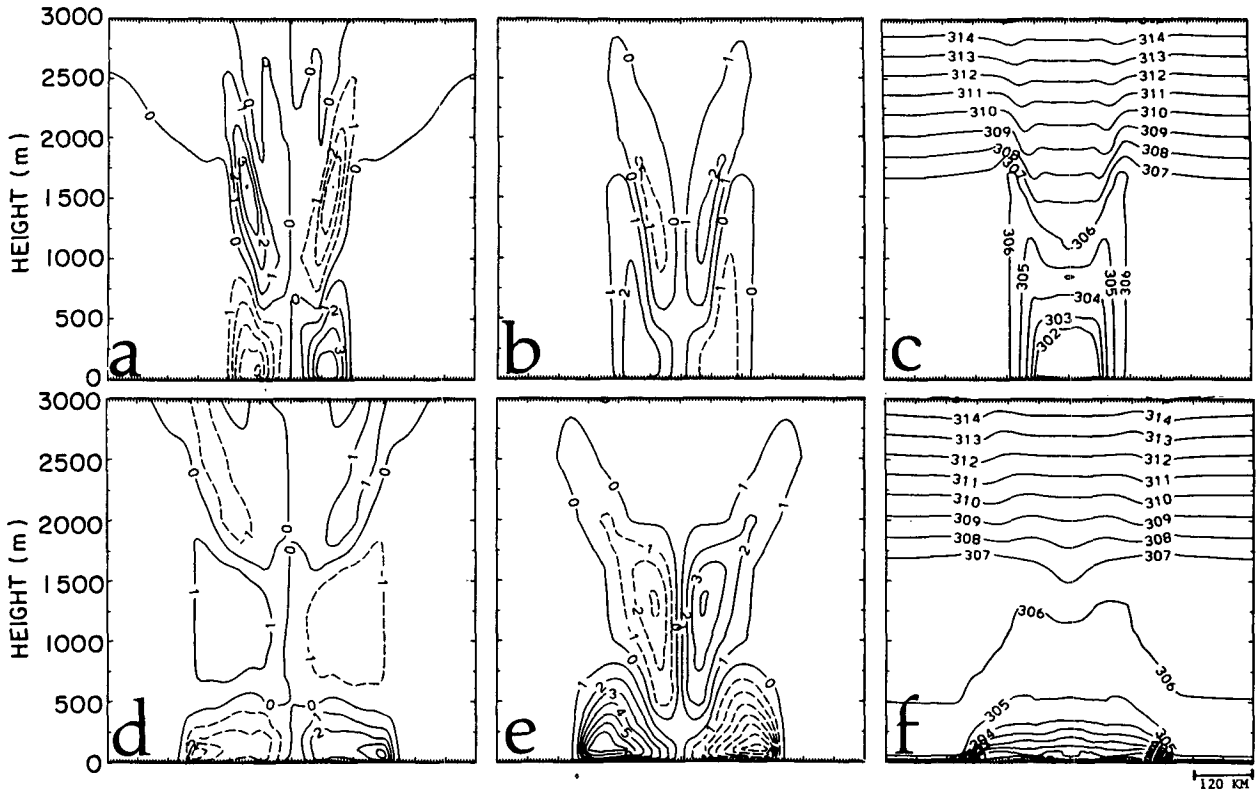

FIG. 9. Simulated x–z fields for case C1: (a) u in meters per second (the flow component from the cool-air pool toward the warm section), (b) v in meters per second (the flow component perpendicular to u), and (c) θ (K) fields along the domain vertical cross section, at 1800 LST, and simulated: (d) u, (e) v, and (f) θ fields along the domain vertical cross section at 2400 LST.

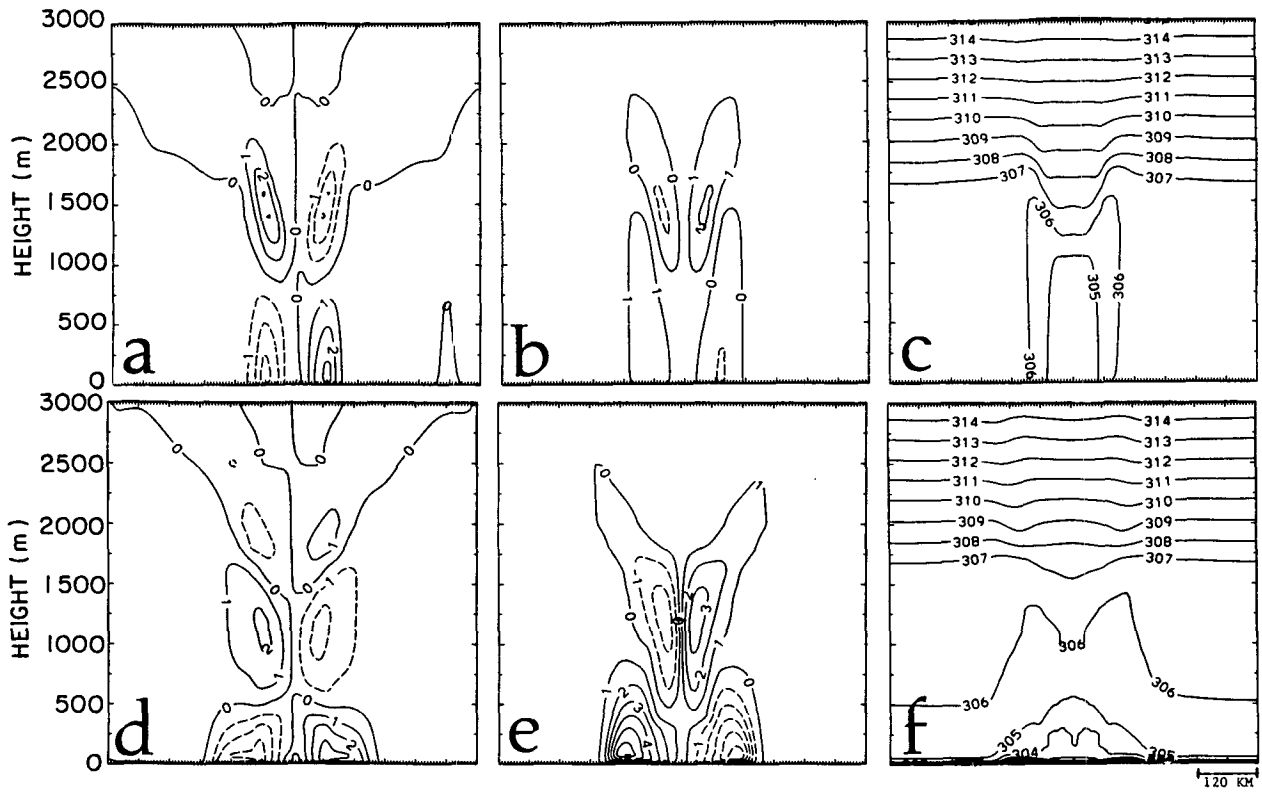

FIG. 10. The same as Fig. 9, except for case C2.

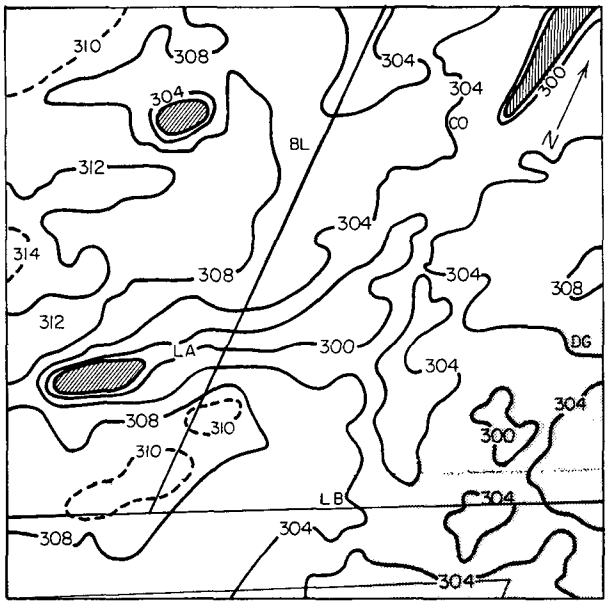

FIG. 11. GOES-IR surface temperature (K) on 14 July 1988 at 1200 MST in a domain including southeast Colorado, southwest Kansas, and northwest Oklahoma, following a precipitation event during the previous day. Line-shaded areas indicate full cloud cover; dot-shaded areas are covered with fair weather cumulus. BL—Burlington; CO—Colby; LA—Lamar; LB—Liberal.

Numerical model evaluations of the importance of daytime surface-moisture availability and spatial variations on the development of a thermally induced circulation are given, for example, in Ookouchi et al. (1984). An observational illustration of this potential forcing is provided in Fig. 11, using the GOES midday surface temperature following a precipitation event of the previous night in southeast Colorado and southwest Kansas. The NWS radar echoes (Fig. 12) suggest that in the area where the lowest daytime surface temperatures were observed, the peak cloud tops were above 13.3 km. Thus, this area apparently was affected by intense precipitation (rain for this area is indicated by the NWS daily precipitation map). Surface temperature variations of $\approx$10 K within relatively short distances are indicated in Fig. 11; following Ookouchi et al. (1984), such observed thermal gradients should lead to a noticeable thermally induced circulation.

When a synoptic flow of 3 m s^{-1} is included (case C3, Fig. 13) the coupling of the thermally induced and synoptic flows causes local intensification of the resultant flow when contrasted with the convergence zones associated with the light wind simulations. The thermal stratification shows similar features as simulated in C1, although the entire thermal structure is shifted somewhat downwind by the background flow.

Figure 14 presents the simulated flows for the winter case (case C4, which is analogous to case C1). Here the initial temperature perturbation was assumed to be smaller compared to that for summer (due to lower background temperature and water-vapor deficit). In addition, the thermal forcing related to the surface differential heating (resulted by the surface moisture availability differentiation) in the winter is smaller. Therefore, in general, the simulated winter circulations were weaker although they showed similar features to those presented for the summer (case C1).

b. Nighttime simulations

These simulations commenced at 2000 LST and used the same initial conditions as in the simulations initiated at noon. During nighttime, unlike daytime, no significant effect is found from the thermal forcing due to ground wetness variations, while the thermal stratification is only affected within a shallow layer (as a result of the net radiative cooling). Figure 15 illustrates the development of the induced circulation in case C5. Six hours following the commencement of the simulation (0200 LST), a shallow circulation (compared to that presented in case C2) is found. The reduced vertical development is attributed to the lack of generation of a convective ABL as in case C2. It is similar to the pattern found for a sea breeze in which the circulations for stable background stability are relatively shallow (e.g., Atkinson 1981). The u and v components of the flow are noticeably smaller (Figs. 15a,b) when compared to those for case C1, and a lateral spread of the cool air pool while maintaining a shallow depth is simulated by that hour (Fig. 15c).

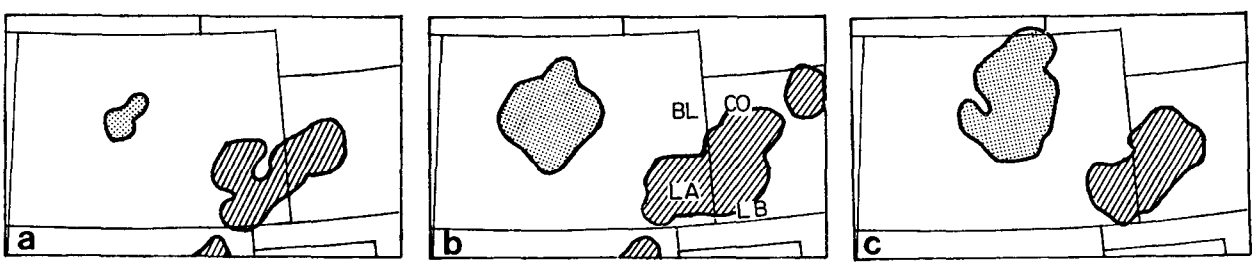

FIG. 12. Areas indicated by the NWS radar to be affected by convective cloud activity during the afternoon and the evening hours of 13 July 1988. Line-shaded areas were associated with peak cloud tops above 13.3 km, dot-shaded areas were associated with peak cloud tops below 13.3 km. (a) 1435 MST; (b) 1835 MST; and (c) 2135 MST.

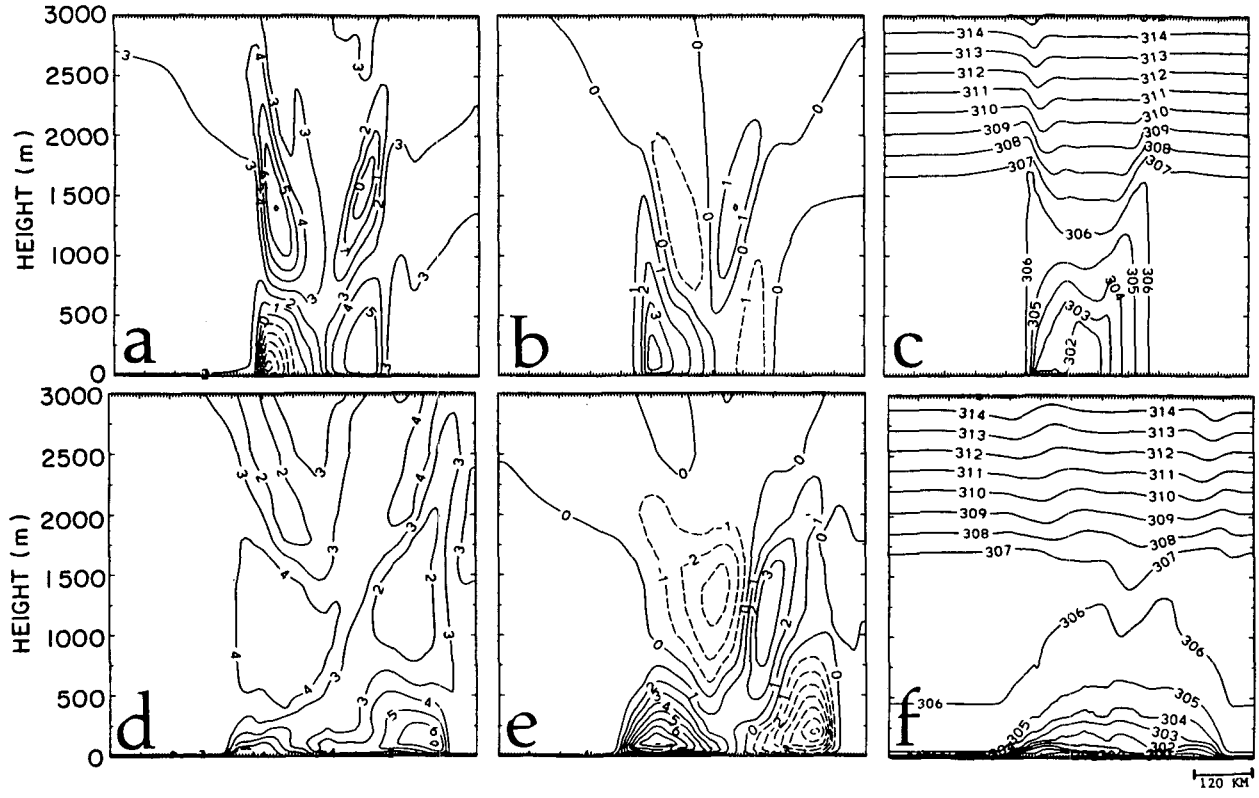

FIG. 13. The same as Fig. 9, except for case C3.

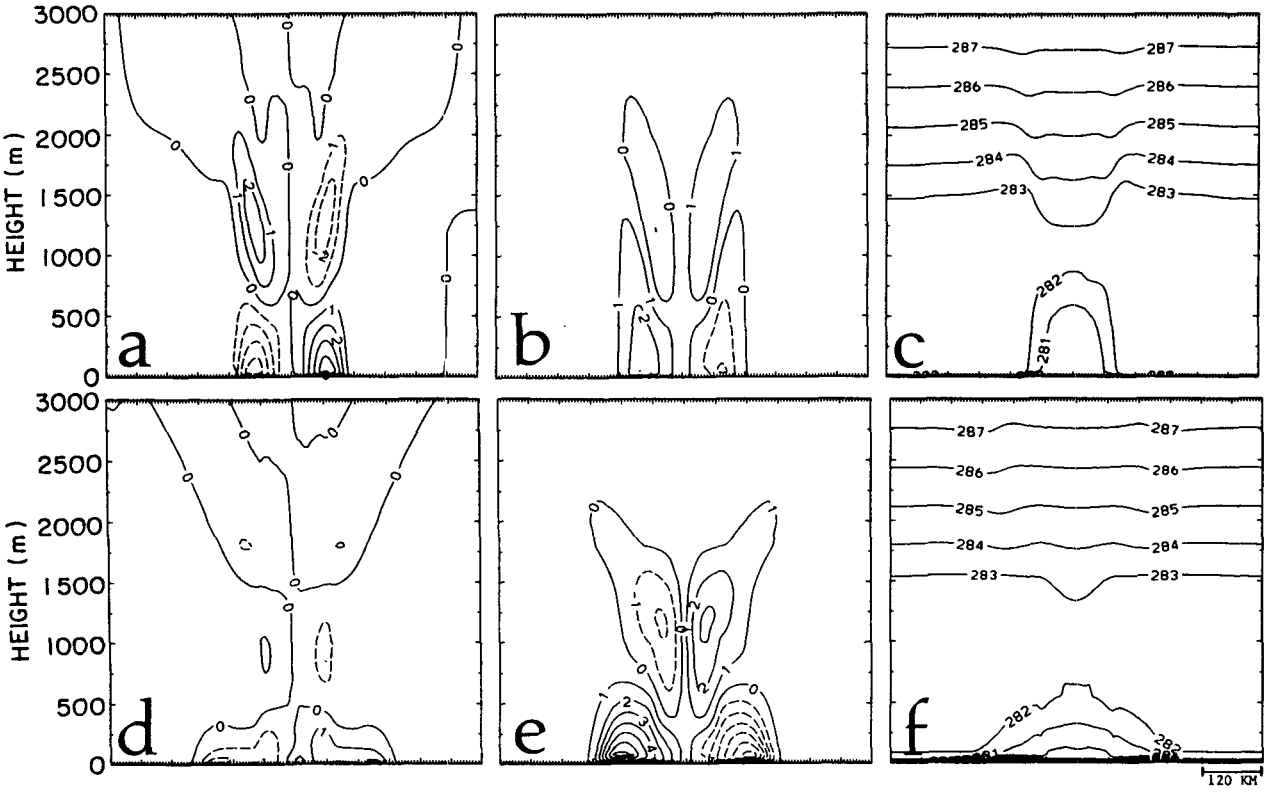

FIG. 14. The same as Fig. 9, except for case C4 (winter case).

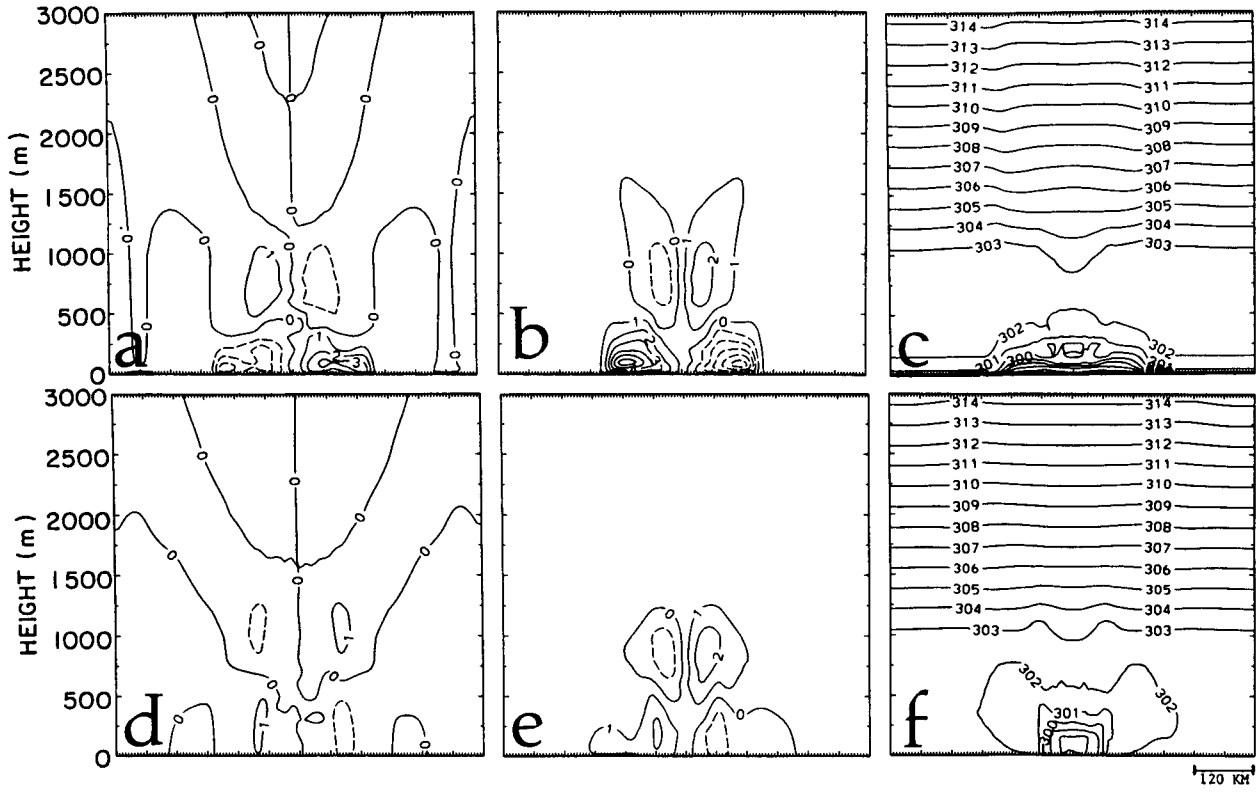

FIG. 15. Case C5. Simulated (a) u, (b) v, and (c) θ fields along the vertical cross section at 0200 LST, and simulated (d) u, (e) v, and (f) θ fields along the vertical cross section at 0800 LST.

During the morning, only light thermally induced winds are simulated (Figs. 15d,e) as a result of the initiation of a convective ABL and increased frictional effects. Finally, case C6 (Fig. 16) provides a simulated nocturnal case as case C5 with a synoptic flow of 3 m s^{-1}; relatively insignificant modifications in the general pattern of perturbation, described for case C5, are involved.

c. *Implications for air pollution*

The simulations of thermal circulations, presented in the previous two subsections, were initialized using typical characteristics of the temperature field in the postprecipitation environment. The characteristics of the thermal circulations were dependent on the period of the day and on the surface wetness conditions in the areas related to the precipitation event. The ABL, in the postprecipitation period over the center of an extensive area affected by precipitation, was poorly developed in vertical extent due to the induced subsidence and the increased surface moisture availability. For occasions with postprecipitation cloudiness, the additional suppression of the surface sensible heat flux is likely to further enhance this feature. The increased flow intensity is likely to offset the thermal stabilization effects on pollutant dispersion. The horizontal thermal contrast associated with the surface cool-air pool will force local thermal circulations similar to those observed in sea-breeze cases. The effects of the sea-breeze circulations on pollutant dispersion are well documented in various studies (e.g., Lyons 1975; Blumenthal et al. 1978; Young and Winchester 1980; Schultz and Warner 1982; Segal et al. 1982; and Lalas et al. 1982, 1987; among others). Therefore, the dispersion characteristics documented for sea breezes can be used to imply general dispersion characteristics for the postprecipitation thermal circulations.

5. Discussion

The impact of precipitation events on the atmospheric ABL and, consequently, on pollutant dispersion characteristics has been evaluated for subtropical and midlatitude locations. The coarse time resolution (12 h) of the routine radiosonde data enabled its usage only in an illustrative manner. Temperature profiles from several field experiments provided more detailed information. Observational evaluations of the lower atmosphere thermal stratification and flow intensity in this study were made based on these data. Additionally, numerical model simulations and scaling estimations were carried out. The evaluations presented in this paper should be considered as preliminary. They do,

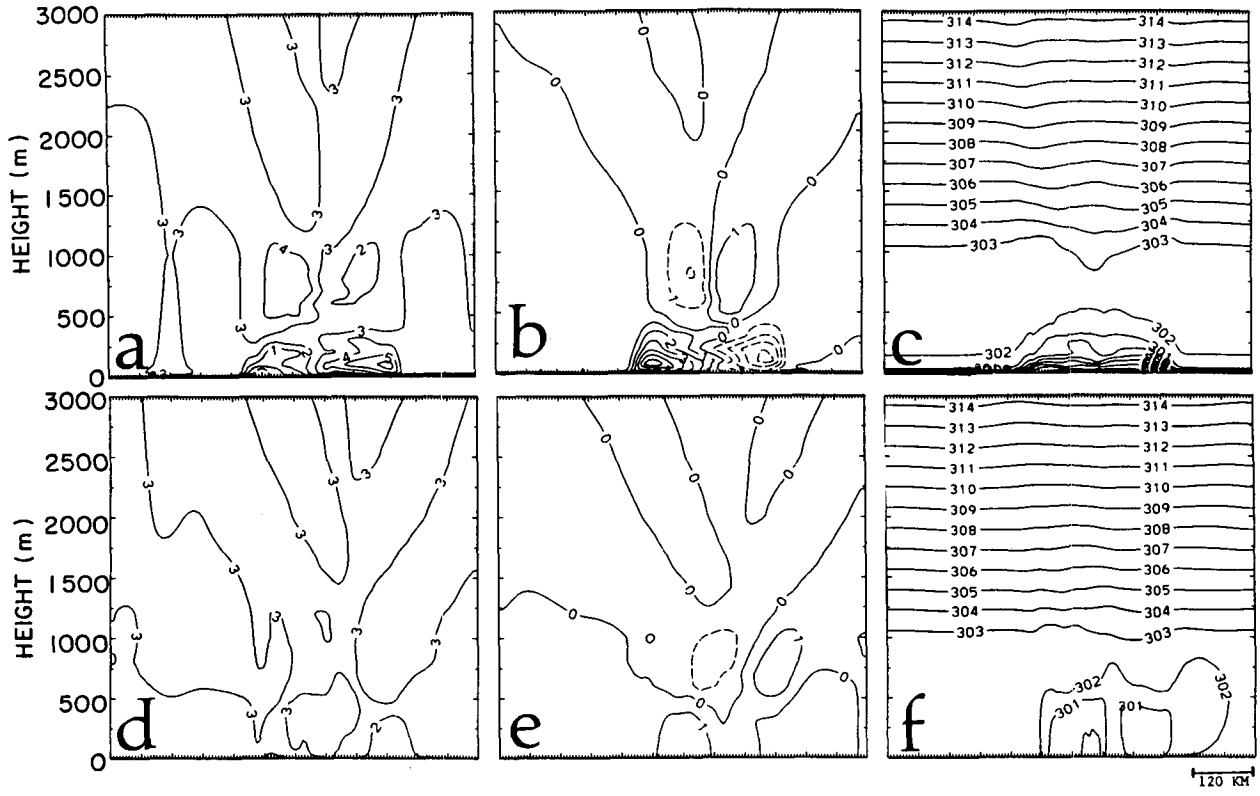

FIG. 16. The same as Fig. 15, except for case C6.

however, suggest the following conceptual model for the meteorological conditions generated in the ABL as a result of precipitation events and their implication to pollutant dispersion:

(i) midlatitude summer convective rain systems result in frequently stable thermal stratification in the lower atmosphere. Occasionally, a near-moist-adiabatic stratification is observed; usually, however, much more intense stable stratification is produced in some portion of the lower atmosphere. Such thermal stratification modifications should lead to the suppression of mechanical turbulence compared to that in the typical convective ABL prior to the rain event. Strong winds usually are induced at least near the storm activity, offsetting the deterioration of the dispersion conditions due to reduced turbulence through enhancement of the ventilation.

(ii) Midlatitude precipitation systems associated with stratiform clouds tend to result in stabilization of the lower atmosphere around the moist adiabatic lapse rate. When these systems are not associated with an intense pressure gradient, strong winds are less likely to prevail. Thus, reduction in the dispersion of pollutants emitted during the precipitation event and, in some period following it, is likely to occur. This implies that a relatively increased contribution to the surface concentrations of near-surface emissions exists. On the other hand, it also implies that a reduction of local contributions to surface concentrations by elevated sources takes place. In the general case, the relative effect of the ventilation and mechanical turbulence on the dispersion can be estimated only following quantification of both processes.

(iii) In precipitation events accompanied by a saturated atmosphere and a moist-adiabatic lapse rate, the turbulent motion is associated with neutral thermal stratification. However, when a saturation deficit is generated, turbulence intensity is reduced as the atmosphere becomes stable. The moist-adiabatic temperature lapse rate depends on the level of the environmental temperature; therefore, variation in the impact, as based on south–north latitudes as well as cold–warm precipitation events, is likely.

(iv) Evaluation of the postprecipitation development of the ABL quantified the strong dependence of its depth on the surface moisture availability and the intensity of the solar radiation. It also indicated the strong dependence of the ABL depth on the background temperature level; lower background temperature is conducive to development of a deeper ABL.

(v) Thermally induced flows due to cooling of the lower atmosphere, following precipitation events, are likely to be more intense in many cases compared to those associated with sea breezes under the same environmental conditions. These circulations also are

supported occasionally by thermal forcing associated with horizontal contrasts in the surface moisture (i.e., wet surface at the area affected by precipitation and dry surface at the area not affected by precipitation). The eroding of the cold air pool, due to the generated thermal circulations, is reduced with time because of the rotation of the flow due to the Coriolis effect (this effect should be most noticeable in the high midlatitudes). The knowledge about the impact of sea breeze on pollutant dispersion may be utilized to further deduce the impact involved with the aforementioned thermal circulations.

Acknowledgments. The study was carried out at CSU and was supported by EPRI under Contract RP-1630-53 and NSF Grant ATM-8616662. R. Arritt, G. Feingold, J. Garratt, J. Schmidt, D. Steyn, and D. Wesley provided useful comments. Computations were carried out at the NCAR Computer Center. We would also like to thank the anonymous reviewer for constructive comments. B. Critchfield and R. Solwa prepared the manuscript.

REFERENCES

Abbs, D. J., and R. A. Pielke, 1986: Thermally forced flow and convergence patterns over northeast Colorado. *Mon. Wea. Rev.*, **114**, 2281–2296.

Atkinson, B. W., 1981: *Mesoscale Atmospheric Circulation.* Academic Press, 495 pp.

Blumenthal, D. L., W. H. White and T. B. Smith, 1978: Anatomy of Los Angeles smog episode: Pollutant transport in the daytime sea-breeze regime. *Atmos. Environ.*, **15**, 893–907.

Briggs, G. A., 1975: Plume rise predictions. *Lectures on air pollution and environmental impact analyses,* D. A. Haugen, Ed., *Amer. Meteor. Soc.*, 59–111.

Carpenter, S. B., T. L. Montgomery, J. M. Leavitt, W. Colbaugh and F. W. Thomas, 1971: Principal plume dispersion models: TVA power plants. *J. Air. Pollut. Contr. Assoc.*, **21**, 491–495.

1968: *Climatic Atlas of the United States.* U.S. Dept. of Commerce, Environmental Data Service, 80 pp.

Fortune, M., 1989: The evaluation of vertical patterns and vortices in mesoscale convective complexes. Ph.D. thesis, Colorado State University, Fort Collins, CO, 183 pp.

Fujita, T., 1955: Results of detailed synoptic studies of squall lines. *Tellus,* **7**, 405–436.

Garratt, J. R., W. L. Physick, R. K. Smith and A. J. Troup, 1985: The Australian summertime cool change. Part II: Mesoscale aspects. *Mon. Wea. Rev.*, **113**, 202–223.

Haagenson, P. L., 1979: Meteorological and climatological factors affecting Denver air quality. *Atmos. Environ.*, **13**, 79–85.

Hamilton, P. J., and R. H. Johnson, 1987: Observations of a midlatitude squall line boundary layer wake. Atmospheric Science paper #414, CSU, Fort Collins, CO, 93 pp.

Hanna, S. R., and R. S. Paine, 1989: Hybrid plume dispersion model (HPDM) development and evaluation. *J. Appl. Meteor.*, **28**, 206–224.

Holzworth, G. C., and R. W. Fisher, 1979: Climatological summaries of the lower few kilometers of radiosonde observations. EPA-600/4-79-026, EPA/ESRL, Research Triangle Park, NC, 141 pp.

Iribarne, J. V., and W. L. Godson, 1981: *Atmospheric Thermodynamics.* Reidel, 259 pp.

Johnson, R. H., and P. J. Hamilton, 1988: The relationship of surface features to the precipitation and airflow structure of intense midlatitude squall lines. *Mon. Wea. Rev.*, **116**, 1444–1472.

Lalas, D. P., V. Veirs, G. Karras and G. Kallos, 1982: An analysis of the SO_2 concentration levels in Athens, Greece. *Atmos. Environ.*, **16**, 531–544.

——, M. Tombrou-Tsella, M. Petrakis, D. N. Asimacopoulos and C. Helmis, 1987: An experimental study of the horizontal and vertical distribution of ozone over Athens. *Atmos. Environ.*, **21**, 2681–2693.

Lyons, W. A., 1975: Turbulent diffusion and pollutant transport in shoreline environments. *Lectures on air pollution and environmental impact analysis,* D. A. Haugen, Ed., AMS, 131–208 pp.

Mahrer, Y., and R. A. Pielke, 1977: A numerical study of airflow over irregular terrain. *Contrib. Atmos. Phys.*, **50**, 98–113.

Mahoney, W. P., 1988: Gust front characteristics and kinematics associated with interacting thunderstorm outflows. *Mon. Wea. Rev.*, **116**, 1474–1491.

McNider, R. T., and R. A. Pielke, 1981: Diurnal boundary-layer development over sloping terrain. *J. Atmos. Sci.*, **38**, 2198–2212.

Monteith, J. L., 1981: Evaporation and surface temperature. *Quart. J. Roy. Meteor. Soc.*, **107**, 1–27.

Ookouchi, Y., M. Segal, R. Kessler and R. A. Pielke, 1984: Evaluation of soil moisture effects on the generation and modification of mesoscale circulations. *Mon. Wea. Rev.*, **112**, 2281–2292.

Penman, H. L., 1956: Evaporation: An introductory survey. *Neth. J. Agric. Sci.*, **4**, 9–29.

Schultz, P., and T. T. Warner, 1982: Characteristics of summertime circulation and pollutants ventilation in the Los Angeles Basin. *J. Appl. Meteor.*, **31**, 672–682.

Segal, M., R. T. McNider, R. A. Pielke and D. S. McDougal, 1982: A numerical model simulation of the regional air pollution meteorology in the Greater Chesapeake Bay area—summer case study. *Atmos. Environ.*, **16**, 1381–1397.

——, W. E. Schreiber, G. Kallos, J. R. Garratt, A. Rodi, J. Weaver and R. A. Pielke, 1989a: The impact of crop areas in northeast Colorado on midsummer mesoscale thermal circulations. *Mon. Wea. Rev.*, **117**, 809–825.

——, J. R. Garratt, G. Kallos and R. A. Pielke, 1989b: On the impact of wet soil and wet canopy temperatures on daytime ABL growth. *J. Atmos. Sci.*, **46**, 3673–3684.

——, X. Jia, Z. Ye and R. A. Pielke, 1990: On the effect of daytime surface evaporation on pollution dispersion. *Atmos. Environ.*, **24A**, 1801–1811.

Steyn, D. G., and I. G. McKendry, 1988: Quantitative and qualitative evaluation of three-dimensional mesoscale numerical model simulation of a sea breeze in complex terrain. *Mon. Wea. Rev.*, **116**, 1914–1926.

Tennekes, H., 1973: A model for the dynamics of inversion above the convective boundary layer. *J. Atmos. Sci.*, **30**, 558–567.

Wakimoto, R. M., 1982: A life cycle of thunderstorm gust fronts as viewed with Doppler radar and rawinsonde data. *Mon. Wea. Rev.*, **110**, 1060–1082.

Wesley, D., and R. A. Pielke, 1990: Observations of blocking-induced convergence zones and effects on precipitation in complex terrain. *Atmos. Res.*, **25**, 235–276.

Young, G. S., and J. W. Winchester, 1980: Association of nonmarine sulfate aerosols with sea-breeze circulation in Tampa Bay. *J. Appl. Meteor.*, **19**, 419–425.

Zipser, E. J., 1977: Mesoscale and convective scale downdrafts as distinct components of squall-line structure. *Mon. Wea. Rev.*, **105**, 1568–1589.